Journal of Medicinal Chemistry



Article

# Use of Structure-Based Drug Design Approaches to Obtain Novel Anthranilic Acid Acyl Carrier Protein Synthase Inhibitors

Diane Joseph-McCarthy, Kevin Parris, Adrian Huang, Amedeo Failli, Dominick Quagliato, Elizabeth Glasfeld Dushin, Elena Novikova, Elena Severina, Margareta Tuckman, Peter J. Petersen, Charles Dean, Christian C. Fritz, Tova Meshulam, Maureen DeCenzo, Larry Dick, Iain J. McFadyen, William S. Somers, Frank Lovering, and Adam M. Gilbert

*J. Med. Chem.*, **2005**, 48 (25), 7960-7969• DOI: 10.1021/jm050523n • Publication Date (Web): 16 November 2005



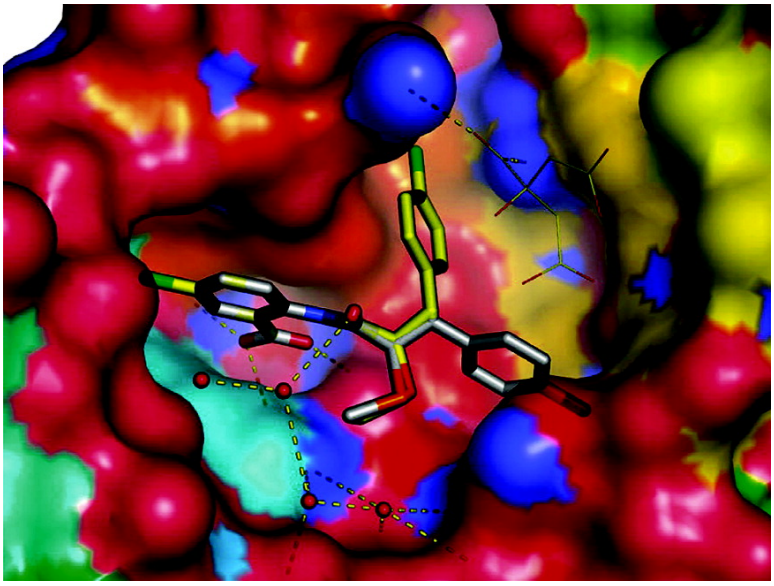

## More About This Article

Additional resources and features associated with this article are available within the HTML version:

- Supporting Information
- Access to high resolution figures
- Links to articles and content related to this article
- Copyright permission to reproduce figures and/or text from this article

View the Full Text HTML

# Use of Structure-Based Drug Design Approaches to Obtain Novel Anthranilic Acid Acyl Carrier Protein Synthase Inhibitors

Diane Joseph-McCarthy,*,† Kevin Parris,† Adrian Huang,† Amedeo Failli,‡ Dominick Quagliato,‡ Elizabeth Glasfeld Dushin,§ Elena Novikova,§ Elena Severina,§ Margareta Tuckman,§ Peter J. Petersen,§ Charles Dean,§ Christian C. Fritz,|| Tova Meshulam,|| Maureen DeCenzo,|| Larry Dick,|| Iain J. McFadyen,† William S. Somers,† Frank Lovering,† and Adam M. Gilbert§

*Wyeth Research, 200 CambridgePark Drive, Cambridge, Massachusetts 01240, Wyeth Research, CN-8000, Princeton, New Jersey 08852, Wyeth Research, 401 North Middleton Road, Pearl River, New York 10945, and Millennium Pharmaceuticals, Inc., 75 Sidney Street, Cambridge, Massachusetts 02139*

*Received June 3, 2005*

Acyl carrier protein synthase (AcpS) catalyzes the transfer of the 4′-phosphopantetheinyl group from the coenzyme A to a serine residue in acyl carrier protein (ACP), thereby activating ACP, an important step in cell wall biosynthesis. The structure-based design of novel anthranilic acid inhibitors of AcpS, a potential antibacterial target, is presented. An initial high-throughput screening lead and numerous analogues were modeled into the available AcpS X-ray structure, opportunities for synthetic modification were identified, and an iterative process of synthetic modification, X-ray complex structure determination with AcpS, biological testing, and further modeling ultimately led to potent inhibitors of the enzyme. Four X-ray complex structures of representative anthranilic acid ligands bound to AcpS are described in detail.

## Introduction

Acyl carrier proteins (ACP) play a vital role in the biosynthesis of fatty acids and other biomolecules in all organisms through the mediation of acyl group transfers.[1] Typically consisting of 80−100 residues, ACP are converted from the inactive *apo* form to the active *holo* form by posttranslation transfer of a 4′-phosphopantetheinyl (4′-PP) moiety from coenzyme A (CoA) to a conserved serine residue in the ACP (Ser36 in *Escherichia coli* ACP).[2] See Figure 1. This reaction is mediated by holo-(acyl carrier protein) synthases (AcpS), which typically contain ∼120 residues. High-resolution crystal structures of AcpS, AcpS + CoA, and AcpS + ACP from *Bacillus subtilis*[3] as well as AcpS and AcpS complexed with 3′5′-adenosine diphosphate (ADP) from *Streptococcus pneumoniae*[4] have shown that AcpS functions as a trimer of three identical monomers, with three identical active sites at each of the monomer−monomer interfaces.

ACP occurs in two main classes, based on the architecture of the system.[5] Type I, or associated, ACP occurs as an integrated domain in a multifunctional protein and is found in mammals, fungi, and certain mycobacteria. Type II, or dissociated, ACP occurs as an independent protein in a nonaggregated multienzyme system and is found in plants and most bacteria. It has been shown that the activation of ACP by AcpS is an essential step in the bacterial biosynthesis of lipopolysaccharides and membrane lipids through genetic studies of *E. coli*[6] and *Streptococcus pneumoniae*.[7] Thus, AcpS has been considered a promising antibacterial target.

This paper describes the structure-based design of novel anthranilic acid AcpS inhibitors. We have previously reported on the combinatorial synthesis and testing of a related series of inhibitors.[8] The identification and optimization of a high-throughput screening (HTS) lead is presented. The optimization process involved modeling of the initial lead into an available AcpS X-ray structure, the design and synthesis of proposed improved compounds, biological testing, and further structure determination, ultimately leading to potent inhibitors of the enzyme. The determination of four X-ray complex structures of representative inhibitors bound to AcpS is detailed, and an analysis of the structures is discussed.

## Results and Discussion

**Biological Data.** An HTS for inhibitors of *B. subtilis* AcpS identified a number of anthranilic acids as leads, with **0** and **4** being representative of them. Both of these compounds had a relatively weak $IC_{50}$ against *B. subtilis* AcpS (12.7 and 32.3 $\mu$M, respectively; see Table 1 and Figure 2). **4** was taken as the initial lead because of its relative novelty and perceived greater potential for optimization.

**4** subsequently also demonstrated measurable minimum inhibitory concentrations (MICs) (32−64 $\mu$g/mL) against a number of Gram-positive organisms (Table 2). Two different assays were implemented to determine if the observed antibacterial activity seen was linked to the inhibition of AcpS. The first, a membrane-damage assay, addressed whether antibacterial activity might instead be attributed to the disruption of the membrane rather than the inhibition of AcpS. **4** was shown to cause rapid cell death of *B. subtilis* at its MIC (90% of cells appeared dead after a 5-min incubation). Because we presumed that specific inhibition of AcpS would not be cidal in such a short time frame, the MIC of **4** most

* Author to whom correspondence should be addressed. E-mail: djoseph@wyeth.com. Phone: 617-665-5627. Fax: 617-665-5682.
† Wyeth Research, Massachusetts.
‡ Wyeth Research, New Jersey.
§ Wyeth Research, New York.
|| Millennium Pharmaceuticals, Inc.

10.1021/jm050523n CCC: $30.25 
Published on Web 11/16/2005

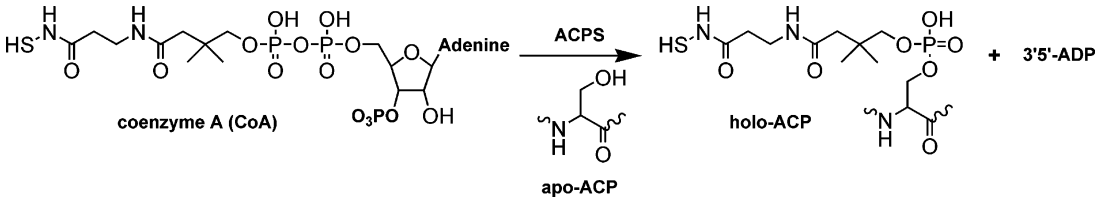


**Figure 1.** Reaction catalyzed by AcpS.

**Table 1.** Summary of $IC_{50}$ Data for Anthranilic Acid Derivatives

| Compound ID | Structure | $IC_{50}$ (μg/mL)[a] | $IC_{50}$ (μM)[a] |
|---|---|---|---|
| **0** | 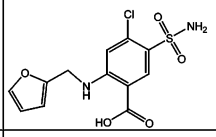 | 4.2 | 12.7 |
| **4** | 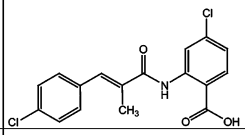 | 11.3 | 32.3 |
| **10** | 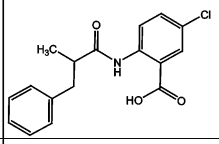 | 0.9 | 2.8 |
| **16** | 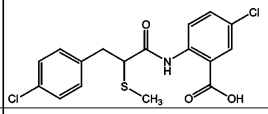 | 0.55 | 1.4 |
| **7** | 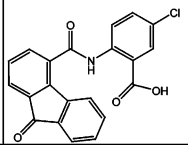 | 0.31 | 0.82 |

[a] Activities of compounds in the HTRF assay.

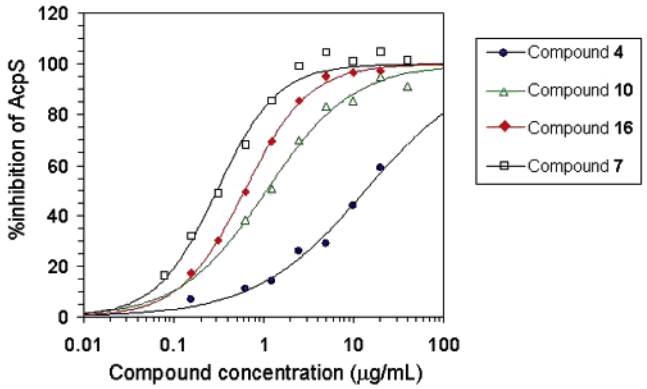


**Figure 2.** Concentration−response curves for select anthranilic acid derivative inhibitors of AcpS. Assays were performed as described in Methods. Data plotted are an average of two replicates.

likely arises from a disruption of the cell membrane, an undesirable property in the development of target-specific antibacterial agents.

The structure-based approach described below led to the design and synthesis of a number of derivatives of **4** with the aim of improving its potency and properties. One of the more potent analogues, **16**, had a 30-fold lower $IC_{50}$ in the AcpS biochemical assay (1.4 μM or 0.55 μg/mL) and did not display any of the membrane-damaging liabilities of the initial lead, **4**. **16** had MICs equivalent to those of **4** (Table 2), but relatively little membrane damage was detected after a 5-min incubation at its MIC (64 μg/mL) with *B. subtilis* PY79 (approximately 20% dead after 5 min. incubation compared to 5% dead in an untreated culture).

For a direct detection of inhibition of AcpS within *B. subtilis*, the relative populations of apo- and holo-ACP were examined by Western blotting mid-logarithmic growth phase cultures. The apo and holo forms of ACP can be distinguished on a polyacrylamide gel containing moderate levels of urea (Figure 3). In Figure 3, two bands can be seen for the monomers of apo- and holo-ACP. This is likely due to the fact that the N-terminal methionine of *B. subtilis* ACP is not completely processed, resulting in a mixed population of ACP.[9] An intense band approximately one-third down the gel is consistent with the homodimer of holo-ACP, which forms during sample preparation, identified in reference 13. In untreated cells, almost all of the ACP pool has been phosphopantetheinylated and exists either as holo-ACP or as holo-ACP with various extensions off of the phosphopantetheine arm that arise during lipid metabolism (lane 1, Figure 3). Under conditions of AcpS underexpression (J. Hixon, unpublished data), apo-ACP accumulates with concomitant reduction in the density of holo-ACP. After incubation of *B. subtilis* PY79 with as little as 4 μg/mL **16**, there was a clear accumulation of apo-ACP (Figure 3), and at 8 μg/mL **16**, there is nearly complete inhibition of AcpS. Given that the accumulation of apo-ACP has previously been shown to be toxic to cells,[13] the apparent reduction in the total ACP pool (unmodified and modified), seen in Figure 3, lane 5, could possibly be the result of feedback control on ACP translation. Slight membrane damage could also lead to reduced visible levels of ACP.

**Optimization of the Lead Series through Molecular Modeling.** Modeling suggested modification to the initial HTS anthranilic acid lead, **4**. More than 50 analogues of this lead were modeled into the site. The results of the modeling are summarized in Figure 4. Specifically, the models indicated that shifting the Cl from the 5-position to the 4-position of the anthranilic head piece should improve potency by better filling a hydrophobic pocket, that adding a small donor group at the 5-position would be expected to be favorable, and that the Cl on the benzyl group interacts favorably with Arg53 (largely through polar/electrostatic interactions) (Figure 5). The modeling also showed that removing the double bond was expected to improve the binding affinity and that the R enantiomer was expected to bind preferentially (see Figure 5A for a model of **10**). Fur-

**Table 2.** Enzyme Activity and Antimicrobial Susceptibility[a]

| | | MIC ($\mu$g/mL) | | | | | |
|---|---|---|---|---|---|---|---|
| cmpd | AcpS $IC_{50}$ ($\mu$g/mL) | *B. subtilis 168* | *S. aureus MRSA* | *E. faecalis VRE* | *S. pneumoniae penR* | *E. coli* | *C. albicans* |
| **4** | 1.3 | 32 | 32 | 64 | 32 | >128 | >128 |
| **16** | 0.55 | 64 | 64 | 128 | 64 | >128 | >128 |

[a] Activities of compounds in the HTRF and MIC assays. Strains used are *Bacillus subtilis* 168, methicillin-resistant *Staphylococcus aureus*, vancomycin-resistant *Enterococcus faecalis*, penicillin-resistant *Streptococcus pneumoniae*, *Escherichia coli*, and *Candida albicans*.

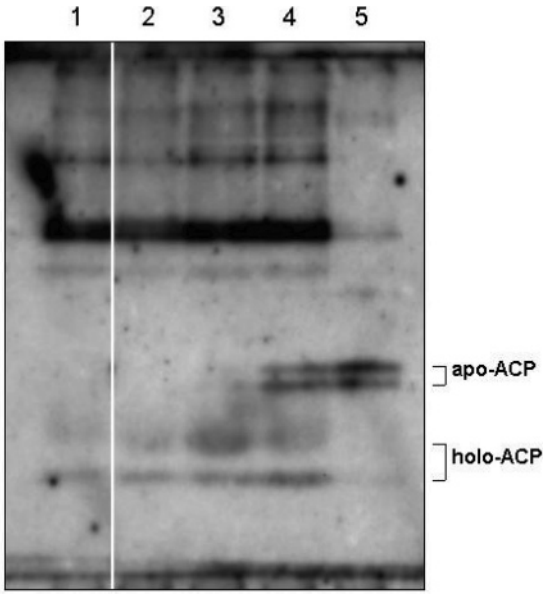


**Figure 3.** Western blot of urea−PAGE with anti-ACP antibodies. *B. subtilis* PY79 cultures were treated with **16**, fractionated on by urea−PAGE, and Western blotted with anti-ACP antibodies. Lane 1 is the no compound control; lanes 2−5 are 1, 2, 4, and 8 $\mu$g/mL, respectively, of **16**.

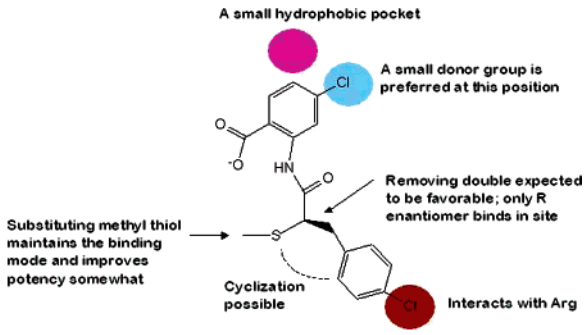


**Figure 4.** Overview of the interactions and opportunities for synthesis determined through molecular modeling.

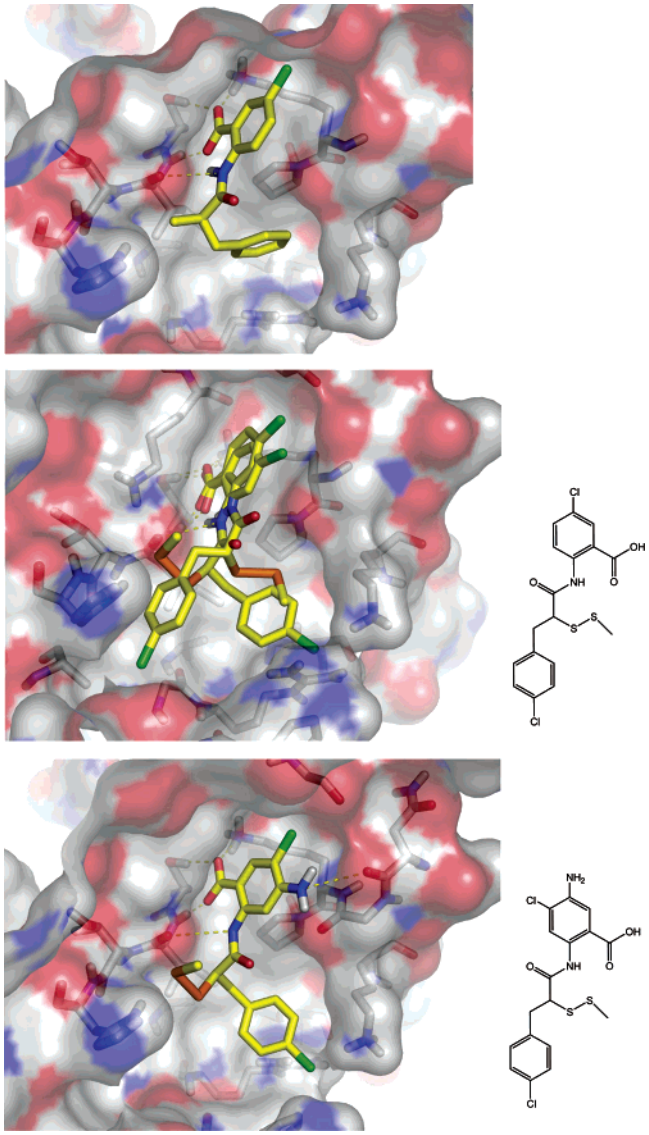

**Figure 5.** Models for proposed compounds bound in the AcpS active site. (A) Model for **10**. (B) Two binding modes for a close analogue of **16** with essentially equivalent energy scores. (C) Proposed analogue with even greater predicted binding affinity.

thermore, replacing the methyl group with a methyl thiol group or disulfide was predicted to have a small favorable effect on potency and maintain the overall binding mode. Modeling of a close analogue of **16** (shown in Figure 5B) showed that only the R enantiomer docked and that two alternate conformations for the chloro benzyl group were likely. There was interest in potentially introducing a disulfide at this position to allow for dynamic combinatorial synthesis of a large number of compounds to explore the unoccupied region of the binding site;[10,11] this approach, however, was not pursued further. Modeling also predicted that cyclizing to connect the methyl group to the benzyl ring (as in **7**) would be favorable and maintain the overall binding mode. Synthesis and testing of **7**, **10**, and **16** confirmed the predictions. Subsequently, the X-ray structure of **16** bound to AcpS confirmed the predicted binding modes; in the structure, described below in detail, only the R enantiomer of the compound was bound, and as predicted, two alternate conformations for the chloro benzyl group were observed.

**X-ray Crystal Structures of Ligand−AcpS Complexes.** The structures of AcpS in complex with the small-molecule inhibitors **0**, **4**, **7**, and **16** have been determined (Table 3). As shown in prior work,[3,4] AcpS exists in a trimeric state with three active sites; each active site is at a dimer interface (see Figure 6 for an illustration of the **4**−AcpS structure). In general, the

**Table 3.** Refinement Statistics

| | AcpS + Cpd **0** | AcpS + **4** | AcpS + **7** | AcpS + **16** |
|---|---|---|---|---|
| space group | *R*32 | $P2_12_12_1$ | *P*3 | *P*3 |
| AcpS molecules per asymmetric unit | 1 | 3 | 6 | 6 |
| unit cell | | | | |
| *a* (Å) | 4.297 | 62.553 | 83.475 | 83.674 |
| *b* (Å) | 84.297 | 83.661 | 83.475 | 83.674 |
| *c* (Å) | 140.211 | 85.979 | 112.105 | 106.719 |
| α, *β*, *γ* (deg) | $\alpha = \beta = 90\ \gamma = 120$ | $\alpha = \beta = \gamma = 90$ | $\alpha = \beta = 90\ \gamma = 120$ | $\alpha = \beta = 90\ \gamma = 120$ |
| maximum resolution (Å) | 1.9 | 2.3 | 2.2 | 2.0 |
| $R_{work}$[a] (%) | 18.8 | 23.4 | 21.0 | 21.2 |
| $R_{free}$[b] (%) | 22.9 | 26.8 | 22.9 | 24.7 |
| rms deviations from ideal geometry for bonds (Å) | 0.027 | 0.007 | 0.011 | 0.007 |
| rms deviations from ideal geometry for angles (deg) | 1.81 | 1.23 | 1.62 | 1.27 |
| AcpS residues observed | 1−119 | 1−119 | 1−119 | 1−119 |
| water molecules | 115 | 87 | 330 | 370 |
| other ions | | Cl-, glycerol | citrate | citrate |

[a] $R_{work} = \Sigma||F_{obs}| - |F_{calc}|/\Sigma|F_{obs}|$. [b] $R_{free}$ is equivalent to $R_{work}$ but calculated for a randomly chosen 5% of reflections omitted from the refinement process.

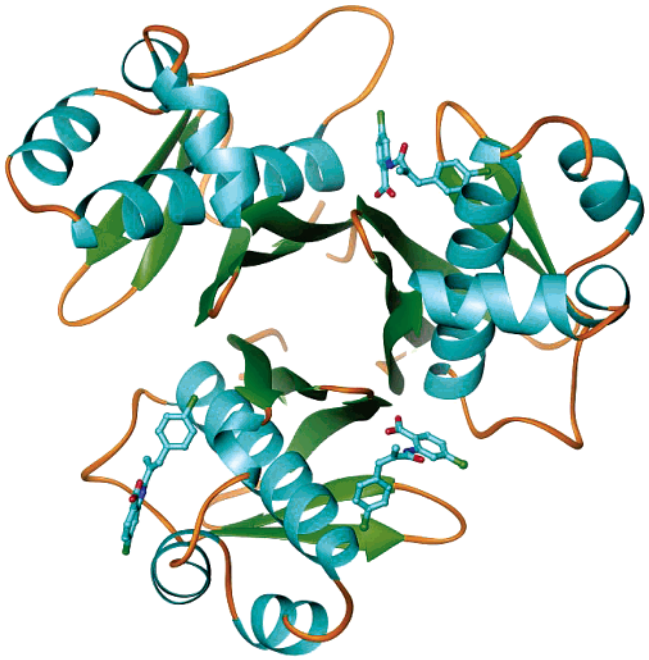

**Figure 6.** Ribbon diagram of the overall structure of the **4**−AcpS complex, showing the catalytic trimer and the position of the bound ligand (colored by element with carbons in cyan) at each dimer interface.

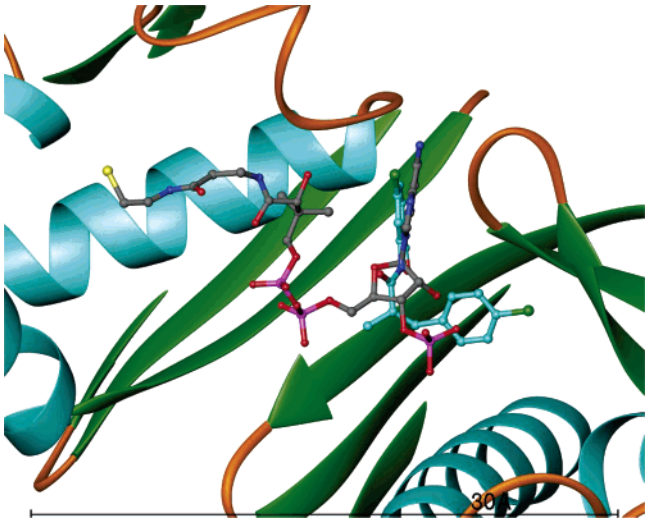

**Figure 7.** Superposition of the **4**−AcpS structure and the CoA−ACPS structure. **4** and CoA are shown colored by element with carbons in cyan for **4** and magenta for CoA. Only protein backbone atoms were superimposed.

anthranilate compounds in the structures presented bind in the AcpS active site where the adenine, ribose, and 3′-phosphate of CoA reside. Hereafter, this site will be referred to as the anthranilate binding site (Figure 7). The inhibitors adopt a U-shape that allows them to sandwich around Pro87 (Figure 8). When referring to residues in the structures, residues in normal text will be from one molecule, whereas those in bold text will be from a second (or symmetry-related) molecule.

**0−AcpS Complex Structure.** In the structure of **0** (a related HTS hit) in complex with AcpS, the asymmetric unit contains only one molecule of AcpS. This molecule of AcpS is positioned on a crystallographic axis such that a *R*32 symmetry operator generates the catalytic trimer. In this structure (Figure 8), the sulfonamide nitrogen is positioned to be within hydrogen-bonding distance to the main-chain carbonyl of Asn84. Additionally, the oxygen atoms of this sulfonamide are adjacent to the main-chain amides of Thr66 and **Gly67**. The phenyl ring of the anthranilate is sandwiched between Lys86, Pro87 of the AcpS molecule and the side chain of **Lys62** of a symmetry-related AcpS molecule. The carboxylic acid is within hydrogen-bond distance to the $N^{\zeta}$ of Lys86, the $O^{\gamma}$ of **Ser102**, and the main-chain N−H of **Ile103**. Aside from a hydrogen bond to a water molecule, the only interaction with the furan ring is a van der Waals (VDW) interaction with Pro87. The final model consists of molecule **0**, a continuous chain involving protein residues 1−119, and 115 water molecules.

**4−AcpS Complex Structure.** The structure of AcpS in complex with **4** contains three molecules of AcpS in the asymmetric unit arranged to form the catalytic trimer. In addition to the three AcpS molecules, the final model contains three molecules of **4**, a glycerol molecule, a chloride ion, and 87 waters. NMR analysis demonstrated that the sample of **4** used for the crystallization experiment was a mixture of cis and trans isomers. Most interestingly, both isomers were found bound to AcpS in this crystal structure. The cis isomer is found in two of the three active sites in the anthranilate binding site. This isomer, like **0**, is held in place by VDW interactions with Lys86, Pro87, and **Lys62**. Additionally, the same interactions exist between the carboxylic acid of the inhibitor and the protein: hydrogen bonds to the $N^{\zeta}$ of

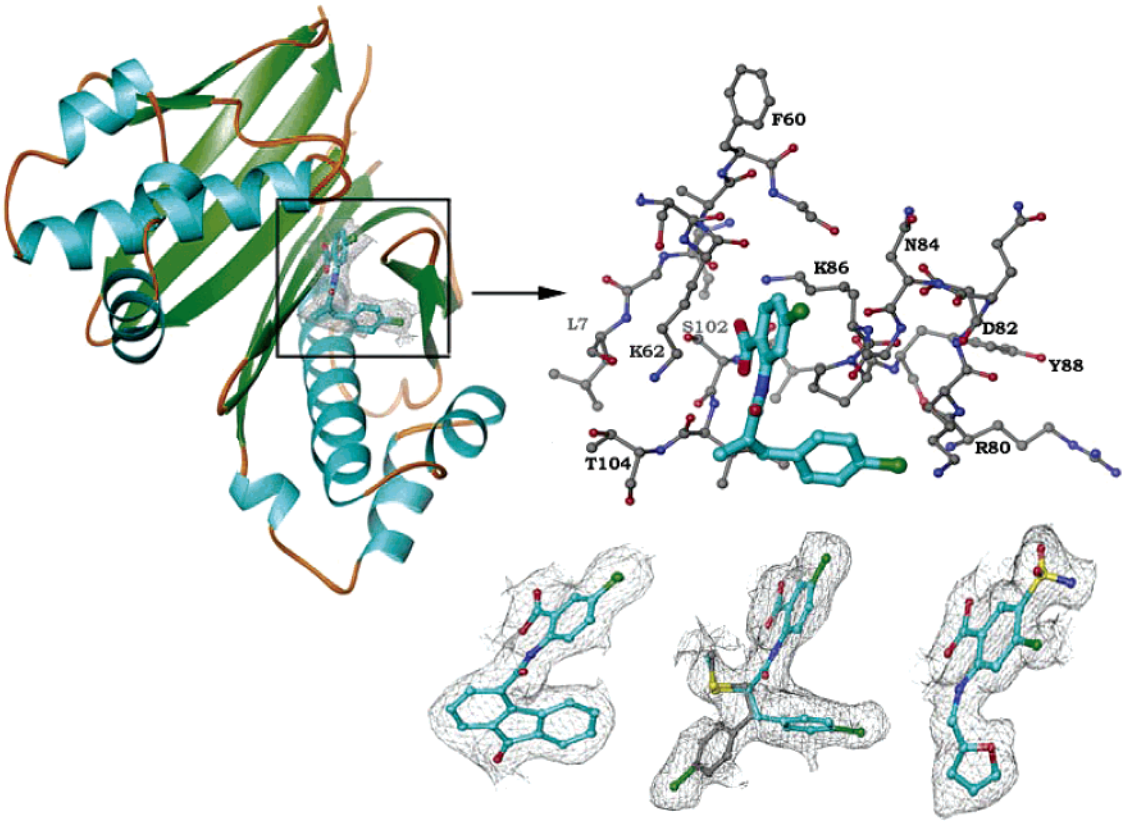


**Figure 8.** Structure of the **4**−AcpS complex is shown with unbiased $2F_o - F_c$ electron density contoured at $1\sigma$ around the ligand. (A) Key protein interactions with the inhibitor are highlighted in the snapshot of the active site. (B) Similar electron density for the ligands in the other three complex structures (**7**, **16**, and **0**).

Lys86, the $O^{\gamma}$ of **Ser102**, and the main-chain N−H of **Ile103**. Adjacent to only one of the molecules of *cis*-**4** is a molecule of glycerol that came from the cryopreservation process prior to data collection. The 1-hydroxyl is positioned to be within hydrogen-bonding distance of the amide carbonyl of the *cis*-**4** molecule. The 3-hydroxyl is within hydrogen-bonding distance of **Gly58** and **Ile68**. The density was unambiguous, but to be certain, we conducted an experiment where the cryopreservation solvent was ethylene glycol rather than glycerol. Examination of the electron density from this experiment showed that the electron density in the area in question had changed and was now consistent with a water molecule. The third active site has no compound in the anthranilate binding pocket but instead has a molecule of the trans isomer. This molecule is found in the active site at the location where the $\beta$-mercaptoethylamine unit of CoA is bound. Additionally, when this structure is superimposed with the structure of the AcpS/ACP complex, this trans molecule overlaps with the positions of the Met44, Val39, and Leu37 side chains of ACP. These ACP residues extend into pockets on AcpS when ACP binds. Specifically, the chloro atom from the anthranilic acid moiety of the trans molecule superimposes with the sulfur of Met44 (ACP), whereas the Leu37 (ACP) side chain coincides with the location of the phenyl ring of the chlorophenyl moiety. Despite these alignments, this binding site is likely to be an artifact of crystal packing as the trans isomer is held into this position by a symmetry-related molecule of AcpS. Supporting the hypothesis of an artifactual binding site is the fact that in the two active sites where the cis isomer binds, the trans binding location is available but is not occupied.

**7−AcpS Complex Structure.** The structure of AcpS in complex with **7** contains six molecules of AcpS in the asymmetric unit. Each of these molecules is placed on a crystallographic three-fold axis, and thus, the catalytic trimer for each is generated by symmetry. In addition to the six AcpS molecules, the final model contains six molecules of **7**, six citric acid molecules, and 330 waters. Each of the **7** molecules is bound in the anthranilate binding pocket with the same contacts as detailed above. In the active site of each AcpS there is also a molecule of citric acid, a component of the crystallization buffer. The citric acid moiety is found ~3.5 Å from **7** and has potential hydrogen bonds to Asp 8, **Lys 62**, and Thr 104.

**16−AcpS Complex Structure.** The structure of AcpS in complex with **16** contains six molecules of AcpS in the asymmetric unit. Like the costructure of AcpS and **7**, each of these molecules is located on a crystallographic three-fold axis; thus, the catalytic trimers for each are generated by symmetry. In addition to the six AcpS molecules, the final model contains six molecules of **16**, six molecules of citric acid, and 370 waters. Each molecule of **16** is bound in the anthranilate binding pocket with the same contacts as detailed above for **4**. Although it is not involved in any substantial contacts with the protein, the thio-methyl group is positioned in the active site so that it coincides with 5′ position of the ribose moiety of CoA. Only the R enantiomer of **16** (a racemic mixture) was observed in the structure. Each active site also indicates that there are electron densities for two alternate conformations for the chloro benzyl

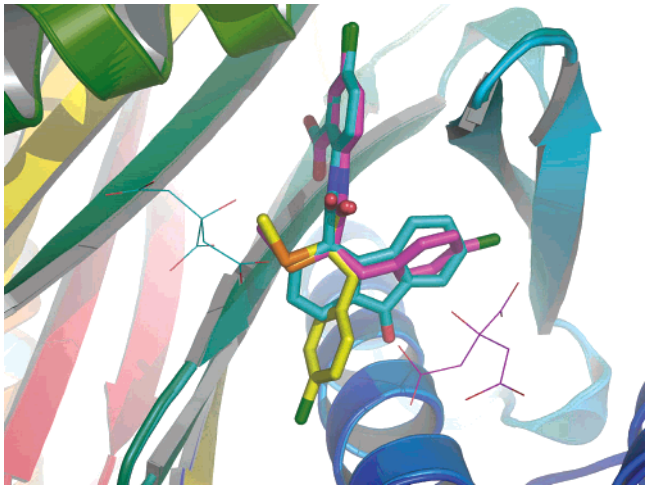

**Figure 9.** Superposition of the **16**−AcpS structure and the **7**−AcpS structure. Only protein backbone atoms (shown in a ribbon representation for each structure) were superimposed. **7** (thick lines) and the corresponding citrate (thin lines) found in the active site are shown colored by element with carbons in cyan. The predicted lower energy mode of the R enantiomer of **16** (thick lines) and the corresponding citrate (thin lines) found near the active site are shown with carbons in magenta; the other observed binding mode for the R enantiomer of **16** (thick lines) is shown with carbons in yellow.

group of **16** (Figure 8). Both binding modes for the chloro benzyl group were expected on the basis of the molecular modeling results. A carbon−carbon bond rotation results in an alternate conformation that gives a more linear molecule rather than one that is U-shaped. This linear rotamer extends the chloro benzyl group into a pocket formed by His105, Gly52, and Glu48.

**Comparison of the Various Complex Structures.** The binding modes for the anthranilic acid portion of each inhibitor in the AcpS protein structure are essentially identical. As expected from the modeling, removing the double bond from **4** improves the binding affinity by allowing the compound to adopt a conformation with a more complementary fit to the protein surface. In the model of **10**, an intermediate in the design process, the Cl at the 5-position fills a small hydrophobic pocket, and the less favorable interaction of Cl at the 4-position with the backbone carbonyl oxygen of Asn85 is removed. **7** and **16** have similar potencies (0.82 and 1.4 $\mu$M, respectively), although the R enantiomer of **16** is expected to have a greater potency than either **7** or the racemic mixture that constitutes **16**. The position of the terminal ring of the tricyclic of **7** overlaps fairly well with the position of the benzyl ring in the predicted lower-energy mode of the R enantiomer of **16** (Figure 9). The carbonyl oxygen on the tricyclic of **7** makes VDW contact with a backbone α-carbon but does not make any polar interactions with the protein and, as such, may not be optimal. The citrate molecule in the active site of structure **7** superimposes with the position of the phosphate group in CoA. **16** clearly could be extended from the position of the sulfur (or **7** from the 3- or 4-positions of the tricyclic) to fill the half of the active site occupied by the phosphopantetheine moiety of CoA. The compounds presented in this paper fill the side of the AcpS active site occupied by the adenine portion of CoA. Because **7** and **16** are both below 385 MW, it should be possible to extend the molecules to further improve their potencies while still maintaining druglike properties.

**Scheme 1**[a]

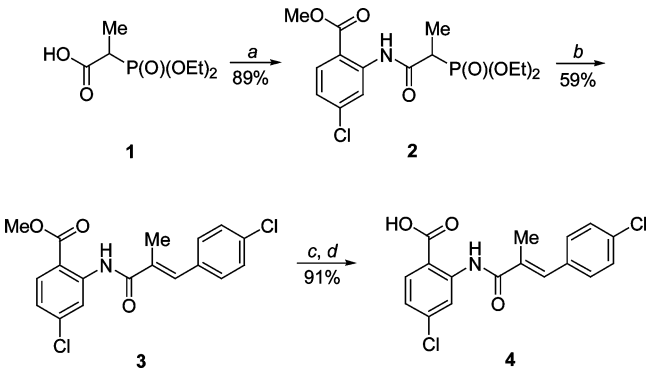


[a] (a) 2-Amino-4-chlorobenzoic acid methyl ester, diisopropylcarbodiimide, cat. DMAP, $CH_2Cl_2$, 23 °C; (b) 4-chlorobenzaldehyde, DBU, LiCl, THF, 23 °C; (c) 1 N LiOH, THF, $H_2O$, 23 °C; (d) 2 N HCl, 23 °C.

**Scheme 2**[a]

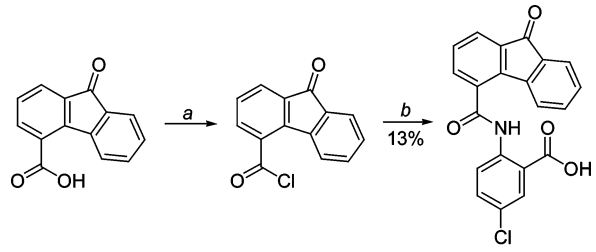


[a] (a) $(COCl)_2$, cat. DMF, PhMe, 23 °C; (b) 2-amino-5-chlorobenzoic acid, toluene, 23 °C.

**Chemistry. 4.** The $^1$H NMR spectrum of the historical sample of **4** showed a mixture of cis and trans double-bond isomers. Thus, the presence of both isomers in the **4**−AcpS complex structure is most likely due to this mixture. Pure *cis*-**4** was prepared as outlined in Scheme 1.

The diethoxyphosphoryl carboxylic acid **1**, prepared according to Krawczyk et al.,[12] was coupled with 2-amino-4-chlorobenzoic acid methyl ester in the presence of 1,3-diisopropylcarbodiimide and catalytic DMAP to give amide **2**. Horner−Emmons coupling with 4-chlorobenzaldehyde in the presence of 1,8-diazabicyclo[5.4.0]-undec-7-ene and lithium chloride in THF gave the cis olefin **3** (100% *E* selectivity determined by HPLC analysis). Saponification of **3** provided the desired *cis*-isomer of **4**.

**7.** This compound was prepared by the coupling of 2-amino-5-chlorobenzoic acid with 9-fluorenone-4-carbonyl chloride (**6**), as shown in Scheme 2.

**10.** α-Methylhydrocinnamic acid **8** is converted to the corresponding acid chloride **9** using oxalyl chloride. This acid chloride is then coupled with methyl 2-amino-5-chlorobenzoate to give the amide, which underwent basic hydrolysis using $LiOH·H_2O$ to give **10** (Scheme 3).

**16** was prepared as shown in Scheme 4. Amino acid **11** was converted to the corresponding α-bromo acid **12** with $NaNO_2$ and KBr in aqueous $H_2SO_4$. Conversion to the amide **14** was effected by conversion to the acid chloride **13** using oxalyl chloride, followed by reaction with methyl 2-amino-5-chloro benzoate. The corre-

**Scheme 3**[a]

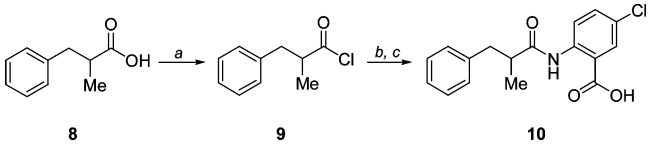

[a] (a) $(COCl)_2$, cat. DMF, $CH_2Cl_2$, 23°C; (b) methyl 2-amino-5-chlorobenzoate, *i*-$Pr_2NEt$, $CH_2Cl_2$, 23 °C; (c) $LiOH \cdot H_2O$, THF/$H_2O$, 23 °C.

**Scheme 4**[a]

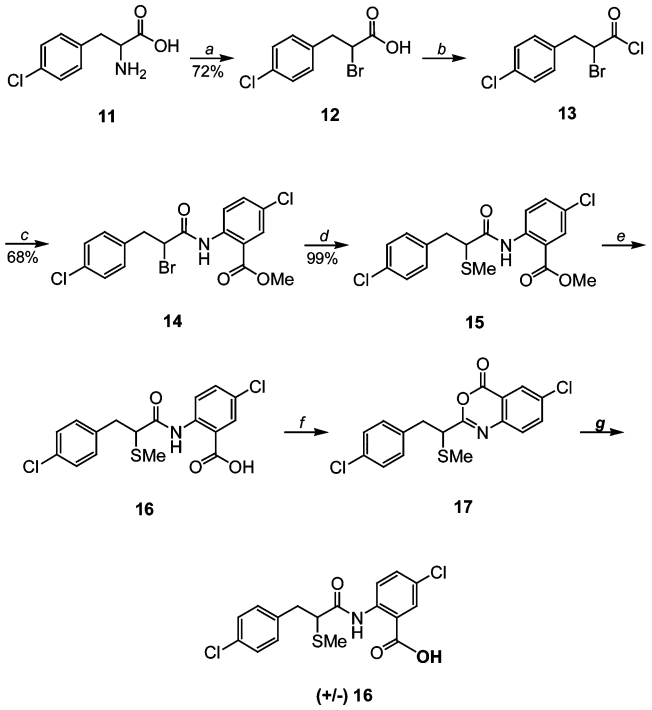

[a] (a) $NaNO_2$, KBr, 1.25 M $H_2SO_4$, −8 to 23 °C; (b) $(COCl)_2$, cat. DMF, $CH_2Cl_2$, 0 to 45 °C; (c) methyl 2-amino-5-chlorobenzoate, pyridine, $CH_2Cl_2$, 23 °C; (d) NaSMe, DMSO, 23 °C; (e) $LiOH \cdot H_2O$, THF/MeOH/$H_2O$, 50 °C; (f) EDCI·HCl, DMAP, $CH_2Cl_2$, 23 °C.

sponding thiomethyl analogue **15** was produced using sodium methylsulfide, and hydrolysis of the methyl ester with $LiOH \cdot H_2O$ gave **16**.

The resolution of **16** by chiral HPLC could not be carried out due to the poor solubility characteristics of the compound. We then attempted the conversion of **16** to the corresponding diastereomeric esters using 1*S*,2*S*,3*S*,5*R*-(+)-isopinocampheol. Under the coupling conditions, only the benzooxazin-4-one **17** was obtained. Successful resolution of **17** was achieved using chiral HPLC; however, subsequent hydrolysis of the individual enantiomers of **17** resulted in complete racemization of the acid formed.

## Conclusions

A series of novel anthranilic acid inhibitors of AcpS, an infectious disease target, were obtained through the use of a structure-based approach for the optimization of a relatively weak HTS lead, **4**. **4** had also been shown to cause cell damage. On a fairly short time scale of less than nine months, **16** was synthesized. The potency of **16** was improved 30-fold over the initial lead, and rapid cell death was not observed in the membrane-damage assay. Molecular modeling and X-ray crystallography together have also clearly delineated opportunities for further optimization of this series of AcpS inhibitors.

## Experimental Section

**Protein Purification for Biological Assays.** The glutathione *S*-transferase (GST) fusion of *B. subtilis* ACP was purified as reported.[3]

**Synthesis of Biotin-CoA.** CoA (Sigma) was dissolved in 0.1 M potassium phosphate, pH 7.2, and mixed with a stoichiometric amount of biocytin maleimide (Molecular Probes, Eugene, OR). The reaction was complete within a few minutes, and aliquots were stored at −20 °C.

**Enzyme Assay.** Enzyme activity was measured using a homogeneous time-resolved fluorescence (HTRF) assay. Assays were run in 384-well plates and consisted of compound, 15 ng/mL AcpS, 1.9 μM biotin−CoA, and 1.25 μg/mL GST−ACP in 50 mM Tris·HCl, pH 8.0, 7.5 mM $MgCl_2$, 3.75 mM DTT, 0.0375% Tween-20, and 37.5 μg/mL BSA in a total volume 20 μL. After 3 h at room temperature, the reaction was terminated by adding 60 μL of the stop/detection mix (82 ng/mL europium cryptate conjugate of GST monoclonal antibody (Packard, Meriden, CT), 28.7 μg/mL streptavidin−allophycocyanin conjugate (ProZyme, San Leandro, CA), 410 mM KF, 4.1 mM EDTA in 0.5 × PBS). The mixture was incubated overnight before reading in a Wallac Victor plate reader (excitation at 340 nm, emission at 665 nm).

**Membrane-Damage Assay.** Molecular Probes' LIVE/DEAD BacLight Kit was used to examine the viability of *B. subtilis* PY79 cultures after incubation with compound. Rapid cell death (within 5 min of treatment) was interpreted as arising from membrane damage induced by the compound rather than due to specific inhibition of AcpS.

**Urea Gel Assay.** The urea−PAGE analysis of ACP is an adaptation of the method found in reference 13. A saturated culture of *B. subtilis* PY79 was diluted 1:200 into Luria−Burtani (LB) medium with compound. The culture was grown to midlogarithmic phase at 37 °C; 0.5 mL was spun down, washed with PBS, and resuspended in 0.5 mL PBS. An equal volume of 10% TCA was added, and proteins were precipitated on ice for 1 h. The precipitate was collected, washed with 1% TCA, and resuspended in 20 μL 1 M Tris. After adding 5 μL loading buffer (100 mM Tris, pH 6.8, 30% glycerol, 0.5 M urea, 0.12 mg/mL bromophenol blue), the sample was fractionated on an 18% polyacrylamide gel containing 1 M urea. Proteins were transferred to an Immobilon-P membrane (Millipore, Bedford, MA) and Western blotted using anti-ACP raised in chicken, rabbit anti-chicken IgG horseradish peroxidase conjugate (Pierce, Rockford, IL), and were developed with Super-Signal West Pico chemiluminescent substrate (Pierce).

**Antimicrobial Susceptibility Testing.** The in vitro activities of the antibiotics were determined by the broth microdilution method as recommended by the National Committee for Clinical Laboratory Standards (NCCLS).[14] Mueller-Hinton II broth (MHBII) (BBL Cockeysville, MD) was the medium employed in the testing procedures. Microtiter plates containing serial dilutions of each antimicrobial agent were inoculated with each organism to yield the appropriate density ($10^5$ CFU/mL) in a 100 μL-final volume. The plates were incubated for 18−22 h at 35 °C in ambient air. The minimal inhibitory concentration for all isolates was defined as the lowest concentration of antimicrobial agent that completely inhibits the growth of the organism as detected by the unaided eye.

**Cocrystallization of AcpS−Inhibitor Complexes.** Histidine-tagged AcpS was purified and concentrated as described earlier.[3] Cocrystals with **0** were obtained by using the hanging drop method with a 10 mg/mL protein solution containing 2 mM **0** equilibrated at 18 °C against 0.2 M potassium dihydrogen phosphate and 20% PEG 3350. Similarly, **4** and **7** were equilibrated against 0.2 M diammonium hydrogen citrate and 20% PEG 3350, whereas **16** was equilibrated against 0.2 M ammonium chloride and 20% PEG 3350.

**Data Collection and Refinement.** Single-wavelength (1.1 Å) data for each inhibitor cocrystal was collected on beamline

5.0.2 at the ALS, Berkeley using an ADSC Quantum-4 CCD detector. A single crystal, cooled to −180 °C, was used for each data set. The data were processed using DENZO and Scalepack.[15]

The structure of the each AcpS/inhibitor complex was solved by molecular replacement using the program AMORE.[16] The probe used in the molecular replacement search was an aggregate of the six monomers of AcpS, as found in the AcpS structure (PDB ID 1F7T), superimposed to yield one "monomer". Prior to refinement, 5% of the data were randomly selected and designated as an $R_{free}$ test set to monitor the progress of the refinement. The structures of each complex were then rebuilt within QUANTA (Accelrys, San Diego, CA) utilizing a series of omit maps. The statistics from refinement are given in Table 3.

**Molecular Modeling of Proposed Compounds.** Confirmed hits from the HTS and proposed compounds were modeled in the AcpS active site using a Monte Carlo docking method. An active site is located at each of the three dimer interfaces in the trimer structure. Starting with the AcpS−CoA X-ray structure,[3] the CoA was removed from each active site, and polar hydrogens were added and optimized using the program CHARMm (Accelrys, San Diego, CA, 2000[17]). An approximately 17 Å-radius spherical region of the protein structure, centered around one of the active sites, was used for the docking calculations. This site file was generated using the program FLO99.[18] The protein was held fixed during the simulations except for the hydroxyl groups of **Ser102** and Ser61. Each ligand or potential ligand was docked into the site by carrying out 1000 mcdock cycles with FLO99. The 25 best poses for each ligand based upon their overall score were retained and viewed graphically. Once the AcpS−**0** complex structure was obtained, a site file for that protein structure was similarly prepared and used for docking all proposed compounds.

The lead compound, **4**, was docked into the AcpS active site as described above, and the binding mode was largely confirmed via X-ray crystallography. Modifications to **4** were modeled, and those that preserved the original binding mode and had improved estimated binding affinities were synthesized.

**4-Chloro-2-[2-(diethoxy-phosphoryl)-propionylamino]-4-methyl-benzoic Acid Methyl Ester (2).** To a 0 °C solution of 2-(diethoxy-phosphoryl)-propionic acid[12] **1** (2.3 g, 10.9 mmol) and 4-(dimethylamino)pyridine (130 mg, 1.09 mmol) in $CH_2Cl_2$ (26 mL) was added 1,3-diisopropylcarbodiimide (0.96 mL, 10.9 mol). After 30 min, methyl 4-chloro-2-amino benzoate (3.04 g, 16.4 mmol) was added. The mixture was allowed to warm to room temperature for 12 h with stirring. An additional 0.2 equiv of 4-(dimethylamino)pyridine and 1,3-diisopropylcarbodiimide were added, and the stirring continued for another 16 h. The mixture was diluted with EtOAc, and the solution was washed with 2 N HCl, water, saturated sodium carbonate, and brine, dried over anhydrous magnesium sulfate, and evaporated to dryness. The residue was purified by flash chromatography over silica Merck-60, eluting with a gradient (from 1:1 to 8:2) of ethyl acetate in hexane to provide **2** (3.65 g, an 89% yield). $^1$H NMR (DMSO-$d_6$, 400 MHz): $\delta$ 1.22 (m, 6H), 1.34 (m, 3H), 3.36 (m, 1H), 3.88 (s, 3H), 4.05 (m, 4H), 7.28 (d, 1H), 7.97 (d, 1H), 8.51 (s, 1H), and 10.93 (s, 1H); MS [(+)ESI, *m/z*]: 377.9 $[M + H]^+$.

**4-Chloro-2-{[(2*E*)-3-(4-chlorophenyl)-2-methylprop-2-enoyl]amino}benzoic Acid Methyl Ester (3).** To a stirred solution of **2** (3.65 g, 9.68 mmol) in THF (100 mL) was added lithium chloride (0.47 g, 11.1 mmol) and 1,8-diazabicyclo[5.4.0]-undec-7-ene (1.11 mL). After 30 min at room temperature, 4-chlorobenzaldehyde was added (1.9 g, 13.5 mmol), and the stirring was continued for 12 h. The reaction mixture was then diluted with water (80 mL) and extracted with $Et_2O$ (3 × 100 mL). The combined organics were dried over anhydrous magnesium sulfate and evaporated to dryness. The residue, preabsorbed onto a column of silica Merck-60, was flash chromatographed using a gradient (from 2 to 10%) of ethyl acetate in hexane to provide the title compound (1.7 g, a 48% yield) as a white solid, mp 105−106 °C. The sample was 98.3% pure by LC/MS: $t_R$ 2.4 min; 362 $[M - H]^-$, 100% pure by HPLC at 254 nm (Keystone Aquasil C18 column; 2.5 min gradient from 95% 10 mM ammonium acetate to 95% acetonitrile; UV detection at 254 and 214 nm). $^1$H NMR (DMSO-$d_6$, 400 MHz): $\delta$ 2.16 (s, 3H), 3.89 (s, 3H), 7.29 (m, 1H), 7.51 (m, 5H), 8.01 (d, 1H), 8.68 (m, 1H), and 11.37 (s, 1H); MS [(+)ESI, *m/z*]: 363.9 $[M + H]^+$.

**4-Chloro-2-{[(2*E*)-3-(4-chlorophenyl)-2-methylprop-2-enoyl]amino}benzoic Acid (4).** To a 0 °C solution of **3** (2.1 g, 5.78 mmol) in THF (75 mL) was added 1 N aqueous lithium hydroxide (17.3 mL), and the mixture was stirred for 12 h at room temperature. The solvent was removed in vacuo; the residue was treated with water and acidified with 2 N hydrochloric acid (to pH 2). The mixture was extracted with dichloromethane (2×) and ethyl acetate (2×). The combined extracts were dried over anhydrous magnesium sulfate and evaporated to provide a solid (1.97 g). Recrystallization from methanol yielded the title compound (1.83 g, a 91% yield) as a white solid, mp 206−207 °C. HPLC: $t_R$ 2.803 min; purity 100% at 254 nm (Cromolith Monolith column, length 100 mm, 5 min gradient from 10 to 100% acetonitrile in water with 0.1% trifluoroacetic acid; flow rate 4 mL/min; UV detection at 254 nm). $^1$H NMR (DMSO-$d_6$, 400 MHz): $\delta$ 2.16 (s, 3H), 7.24 (m, 1H), 7.5 (m, 5H), 8.03 (d, 1H), 8.78 (s,1H), and 11.93 (s, 1H). *E* stereochemistry supported by NOE data; MS [(−)ESI, *m/z*]: 348.01 $[M - H]^-$. Anal. Calcd for $C_{17}H_{13}Cl_2NO_3$: C 58.31, H 3.74, N 4. Found: C 58.37, N 3.67, N 3.89.

**5-Chloro-2-{[(9-oxo-9H-fluoren-4-yl)carbonyl]amino}-benzoic Acid (7).** To a stirred mixture of 9-fluorenone-4-carboxylic acid **5** (500 mg, 2.2 mmol) and toluene (20 mL) contaning a catalytic amount of DMF, was added oxalyl chloride (312 mg, 2.5 mmol) in drops. After 1 h, a suspension of 2-amino-5-chlorobenzoic acid (421 mg, 2.5 mmol) was added, and the mixture was stirred for 12 h at room temperature. The solvent was removed, and the residue was partitioned between 0.1 N hydrochloric acid and ethyl acetate. The insoluble material was collected, and the organic phase was evaporated to dryness. The evaporated organics and the insoluble solids were combined and triturated with methanol. The resulting yellow solid was collected and dried under vacuum (108 mg, a 13% yield). $^1$H NMR (DMSO-$d_6$, 400 MHz): $\delta$ 7.41 (t, 1H), 7.56 (m, 2H), 7.67 (d, 1H), 7,78 (m, 3H), 7.85 (d, 1H), 7.96 (s, 1H), 8.58 (d, 1H), and 11.67 (s, 1H); MS [(+)ESI, *m/z*]: 376 $[M + H]^+$; RP-HPLC: $H_2O$/MeCN/0.2% TFA: 2.49 min; 97.4%; $H_2O$/MeCN/0.2% $Et_3N$: 3.10 min, 95.1%.

**5-Chloro-2-[(2-methyl-3-phenylpropanoyl)amino]benzoic Acid (10).** To a solution of α-methylhydrocinnamic acid **8** (0.2820 g, 1.72 mmol), a few drops of DMF, and 50 mL $CH_2Cl_2$ was added oxalyl chloride (0.178 mL, 2.06 mmol) dropwise at 23 °C. After stirring at room temperature for 1 h, the mixture was concentrated to dryness. A solution of methyl 2-amino-5-chlorobenzoate (0.318 g, 1.72 mmol), *i*-$Pr_2Et$ (0.191 g, 1.90 mmol), and 15 mL $CH_2Cl_2$ was added dropwise, and the reaction mixture was stirred at room temperature overnight. After dilution with water and extraction with ethyl acetate, the organic extracts were evaporated to provide a yellow oil (0.357 g, 63%), which was treated with $LiOH·H_2O$ (0.45 g, 10.8 mmol) in 20 mL 1:1 THF/$H_2O$. The resulting mixture was stirred overnight at room temperature. The reaction mixture was neutralized to pH 6 by the addition of 1 M aqueous sodium dihydrogenphosphate and then was extracted with EtOAc. The organic extracts were dried over anhydrous $Na_2SO_4$ and evaporated to dryness. The resulting solid was dissolved in a minimum amount of dichloromethane, and the solution was diluted with hexane until a precipitate was formed. The precipitate was collected by filtration to give the title compound (0.345 g, 100%) as a white solid. $^1$H NMR ($CD_3OD$, 300 MHz): $\delta$ 1.19 (d, $J$ = 6.6 Hz, 3H), 2.71 (m, 2H), 2.94 (m, 1H), 7.14 (m, 5H), 7.44 (dd, $J$ = 9.0, 2.7 Hz, 1H), 7.92 (d, $J$ = 2.7 Hz, 1H), and 8.47 (d, $J$ = 9.0 Hz, 1H). MS [(−)ESI, *m/z*]: 316.06 $[M - H]^-$; [(+)ESI, *m/z*]: 318.11 $[M + H]^+$. RP-

HPLC: $H_2O/CH_3CN$/0.1% formic acid: 5.87 min; 99.8%; $H_2O/CH_3OH$/0.1% formic acid: 7.12 min, 100.0%.

**2-Bromo-3-(4-chloro-phenyl)propionic Acid (12).** Into 1.25 M aqueous sulfuric acid (65 mL) at −8 °C was added KBr (11.42 g, 96.0 mmol) followed by 4-chlorophenyl alanine **11** (5.99 g, 30.0 mmol). To this stirred suspension was added sodium nitrite (2.07 g, 30.0 mmol) in portions over a period of 45 min. The mixture was allowed to warm slowly to room temperature for 1 h. The reaction mixture was extracted with EtOAc (3×), and the combined organic extracts were washed with water and brine. The organic phase was dried ($MgSO_4$), filtered, and evaporated to a light-yellow oil that solidified upon standing. The yield of the title compound was 72% (5.69 g). This material was carried on directly to the next step.

**2-[2-Bromo-3-{4-chloro-phenyl)propionylamino]-5-chlorobenzoic Acid Methyl Ester (14).** 2-Bromo-5-(4-chlorophenyl)propionic acid **12** (5.31 g, 20.2 mmol), dichloromethane (30 mL), and DMF (2 drops), under a $N_2$ atmosphere, were cooled to 0 °C and treated with oxalyl chloride (12.8 mL, 0.101 mol). After stirring and warming to room temperature over 2 h, the mixture was placed in an oil bath at 45 °C for 3 h. TLC analysis (aliquot quenched with methanol) showed complete conversion to acid chloride **13**. The mixture was evaporated and then reconstituted with dichloromethane and re-evaporated. This was repeated 3×. The evaporator was filled with dry nitrogen gas when opened. The resulting yellow oil was dissolved in dry dichloromethane and cooled to 0 °C, and pyridine (1.46 g, 18.4 mmol) was added. A solution of methyl 2-amino-5-chlorobenzoate (3.41 g, 18.4 mmol) in dichloromethane (30 mL) was rapidly added in drops, and the mixture was stirred at room temperature for 12 h. The resulting mixture was washed with 0.1 N aqueous HCl (2×), water, and brine. The organic phase was dried ($MgSO_4$), filtered, and evaporated. The title compound was isolated pure by flash chromatography (silica gel, 10% ethyl acetate in hexane) and crystallized from hot hexane/ethyl acetate. The yield of the title compound was 68% (5.90 g). $^1$H NMR ($CDCl_3$, 400 MHz): $\delta$ 11.59 (br s) and 11.43 (br s) (rotamers, 1H), 8.64 (m, 1H), 8.00 (m, 1H), 7.51 (m, 1H), 7.24 (m, 2H), 7.18 (m, 2H), 4.61(m) and 4.52(m) (rotamers, 1H), 3.92 (s, 3H), and 3.58−3.24 (series of m, 2H).

**5-Chloro-2-[3-(4-chloro-phenyl)-2-methylsulfanyl-propionylamino)benzoic Acid Methyl Ester (15).** To a solution of 2-[2-bromo-3-{4-chloro-phenyl)propionylamino]-5-chlorobenzoic acid methyl ester **14** (2.00 g, 4.63 mmol) in DMSO (10 mL) was added sodium methyl sulfide (406 mg, 5.78 mmol). The mixture was stirred at room temperature for 1 h. Water (25 mL) was then added, and the resulting mixture was extracted with ethyl acetate (2 × 50 mL). The combined organic extracts were washed with water and brine, dried ($MgSO_4$), filtered, and evaporated to give a white solid. Recrystallization from hot hexane/ethyl acetate gave 1.84 g (4.62 mmol, a 99% yield) of the title compound as a white crystalline solid, mp 141 °C. $^1$H NMR (DMSO-$d_6$, 400 MHz): $\delta$ 10.78 (br s, 1H), 8.17 (m, 1H), 7.82 (m, 1H), 7.62 (m, 1H), 7.26 (m, 4H), 3.80 (s, 3H), 3.77 (m,1H), 3.14 (m, 1H), 2.91 (m, 1H), and 2.07 (s, 3H). MS (ESI) *m/z*: 398 ([M + H]$^+$); Anal. Calcd for $C_{18}H_{17}NCl_2O_3S$: C 54.82, H 4.30, N 3.52. Found: C 54.34, H 4.24, N 3.17.

**5-Chloro-2-[3(4-chloro-phenyl)-2-methylsulfanyl-propionylamino)benzoic Acid (16).** To 5-chloro-2-[3-(4-chlorophenyl)-2-methylsulfanyl-propionylamino)benzoic acid methyl ester **15** (1.23 g, 2.87 mmol) in 50 mL of THF/$H_2O$/MeOH (5.0/2.5/1.0) was added LiOH·$H_2O$ (902 mg, 21.51 mmol). The mixture was heated in an oil bath at 50 °C for 1 h. The organics were removed by evaporation, water (30 mL) was added and, the pH was adjusted to 4 using 2 N HCl. This mixture was extracted using ethyl acetate (4 × 50 mL). The combined organic extracts were dried ($MgSO_4$), filtered, and evaporated to a white solid. The solid was purified by crystallization from ethanol/water to give 0.625 g (57% yield) of the title compound as a white crystalline solid, mp 173−174 °C. $^1$H NMR (DMSO-$d_6$, 400 MHz): $\delta$ 11.37 (br s, 1H), 8.42 (d, $J$ = 9.03 Hz, 1H), 7.90 (d, $J$ = 2.56 Hz, 1H), 7.64 (dd, $J$ = 9.03 and 2.56 Hz, 1H), 7.31 (m, 4H), 3.79 (t, 1H), 3.18 (m,1H), 2.95 (m, 1H), and 2.09 (s, 3H); MS (ESI) *m/z*: 384 ([M + H]$^+$); *m/z*: 382 ([M − H]$^-$). Anal. Calcd for $C_{17}H_{15}NCl_2O_3S$: C 53.13, H 3.93, N 3.64. Found: C 53.23, H 4.00, N 3.51.

**6-Chloro-2-[2-(4-chloro-phenyl)-1-methylsulfanyl-ethyl]-benzo[*d*][1,3]oxazin-4-one (17).** A mixture of 5-chloro-2-[3(4-chloro-phenyl)-2-methylsulfanyl proprionylamino) benzoic acid **16** (50 mg, 0.130 mmol) and 4-(dimethylamino)pyridine (0.016 g, 0.050 mmol) in $CH_2Cl_2$ (4 mL) at 0 °C was treated with 1-[-3-(dimethylamino)propyl]ethylcarbodiimide HCl (28 mg, 0.148 mmol). The resulting mixture was stirred for 2 h at 23 °C. The $CH_2Cl_2$ was evaporated, and the residue was partitioned between ethyl acetate and water. The organic phase was then washed with aqueous $NaHCO_3$ (2×), water (2×), and brine (1×). The organic phase was dried ($Na_2SO_4$), filtered, and evaporated. The solid was purified using flash chromatography (silica gel, 15−20% gradient of diethyl ether/hexane). Yield: 0.035 g (74%), mp 125 °C. $^1$H NMR (DMSO-$d_6$, 400 MHz): $\delta$ 8.08 (d, $J$ = 2.45 Hz, 1H), 7.95 (dd, $J$ = 2.45 and 8.71 Hz, 1H), 7.64 (d, $J$ = 9.03 Hz, 1H), 7.33 (m, 4H), 4.03 (t, $J$ = 7.9 Hz, 1H), 3.33 (m,1H), 3.11 (m, 1H), and 2.12 (s, 3H); MS (ESI) *m/z*: 366 ([M + H]$^+$); *m/z*: 364 ([M − H]$^-$); Anal. Calcd for $C_{17}H_{13}NCl_2O_2S$: C 55.75, H 3.58, N 3.83. Found: C 55.66, H 3.22, N 3.27.

**Chiral Separation of 17.** Chiral separation was achieved using a preparative Chiralcel AD column (25 cm × 2 cm) using methanol as the mobile phase (12 mL/min). The separated optical antipodes of **17** were then used in the following experiment.

**(±)-5-Chloro-2-[3(4-chlorophenyl)-2-methylsulfanyl-proprionylamino)benzoic Acid (16).** A single optical isomer of 6-chloro-2-[2-(4-chlorophenyl)-1-methylsulfanyl-ethyl]benzo-[*d*][1,3]oxazin-4-one **17** (3.2 mg, 8.33 $\mu$mol) in 250 $\mu$L of THF/water/MeOH, (5.0/2.5/1.0) was treated with LiOH·$H_2O$ (1.1 mg, 24.78 $\mu$mol), and the resulting mixture was stirred at room temperature. TLC showed complete conversion to product in 1.5 h. The mixture was adjusted to pH 6 using 0.1 N aq HCl, and the mixture was extracted with dichloromethane (3 × 10 mL). The combined organic extracts were washed with water (2×), dried ($MgSO_4$), filtered, and evaporated. $^1$H NMR analysis of this material confirmed that **16** was obtained, but chiral HPLC (using a preparative Chiralcel AD column (25 cm × 2 cm) using methanol as the mobile phase (12 mL/min)) showed that complete racemization had occurred.

**Supporting Information Available:** Elemental analysis and HPLC results. This material is available free of charge via the Internet at http://pubs.acs.org.

## References


(1) Magnuson, K.; Jackowski, S.; Rock, C. O.; Cronan, J. E. J. Regulation of fatty acid biosynthesis in *Escherichia coli*. *Microbiol. Rev.* **1993**, *57*, 522−542.

(2) Elovson, J.; Vagelos, P. R. Acyl carrier protein. X. Acyl carrier protein synthase. *J. Biol. Chem.* **1968**, *243*, 3603−3611.

(3) Parris, K. D.; Lin, L.; Tam, A.; Mathew, R.; Hixon, J.; et al. Crystal structures of substrate binding to *Bacillus subtilis* holo-(acyl carrier protein) synthase reveal a novel trimeric arrangement of molecules resulting in three active sites. *Struct. Folding Des.* **2000**, *8*, 883−895.

(4) Chirgadze, N. Y.; Briggs, S. L.; McAllister, K. A.; Fischl, A. S.; Zhao, G. Crystal structure of *Streptococcus pneumoniae* acyl carrier protein synthase: An essential enzyme in bacterial fatty acid biosynthesis. *EMBO J.* **2000**, *19*, 5281−5287.

(5) Prescott, D. J.; Vagelos, P. R. Acyl Carrier Protein. *Adv. Enzymol.* **1971**, *36*, 269−311.

(6) Takiff, H. E.; Baker, T.; Copeland, T.; Chen, S. M.; Court, D. L. Locating essential *Escherichia coli* genes by using mini-Tn10 transposons: The pdxJ operon. *J. Bacteriol.* **1992**, *174*, 1544−1553.

(7) McAllister, K. A.; Peery, R. B.; Meier, T. I.; Fischl, A. S.; Zhao, G. Biochemical and molecular analyses of the *Streptococcus pneumoniae* acyl carrier protein synthase, an enzyme essential for fatty acid biosynthesis. *J. Biol. Chem.* **2000**, *275*, 30864−30872.

(8) Gilbert, A. M.; Kirisits, M.; Toy, P.; Nunn, D. S.; Failli, A.; et al. Anthranilate 4H-oxazol-5-ones: Novel small molecule antibacterial acyl carrier protein synthase (AcpS) inhibitors. *Bioorg. Med. Chem. Lett.* **2004**, *14*, 37−41.

(9) Morbidoni, H. R.; de Mendoza, D.; Cronan, J. E., Jr. *Bacillus subtilis* acyl carrier protein is encoded in a cluster of lipid biosynthesis genes. *J. Bacteriol.* **1996**, *178*, 4794−4800.
(10) Eliseev, A. V.; Lehn, J.-M. Dynamic combinatorial chemistry: Evolutionary formation and screening of molecular libraries. *Curr. Top. Microbiol. Immunol.* **1999**, *243*, 159−172.
(11) Erlanson, D. A.; Braisted, A. C.; Raphael, D. R.; Randal, M.; Stroud, R. M.; et al. Site-directed ligand discovery. *Proc. Natl. Acad. Sci. U.S.A.* **2000**, *97*, 9367−9372.
(12) Krawczyk, H.; Koszuk, J.; Bodalski, R. A Useful Synthesis of Diethyl 1-Substituted Vinylphosphonates. *Pol. J. Chem.* **2000**, *74*, 1123−1128.
(13) Keating, D. H.; Carey, M. R.; Cronan, J. E., Jr. The unmodified (apo) form of *Escherichia coli* acyl carrier protein is a potent inhibitor of cell growth. *J. Biol. Chem.* **1995**, *270*, 22229−22235.
(14) *Methods for Dilution Antimicrobial Susceptibility Tests for Bacteria That Grow Aerobically*; Approved Standards, M7-A5; National Committee for Clinical Laboratory Standards: Wayne, PA, 2000.
(15) Otwinowski, Z.; Minor, W. Processing of X-ray diffraction data collected in oscillation mode. *Methods Enzymol.* **1997**, *276*, 307−326.
(16) Navaza, J. AmoRe: An automated package for molecular replacement. *Acta Crystallogr., Sect. A: Found. Crystallogr.* **1994**, *40*, 157−163.
(17) Brooks, B. R.; Bruccoleri, R. E.; Olafson, B. D.; States, D. J.; Swaminathan, S.; et al. CHARMM: A program for macromolecular energy, minimization, and dynamics calculations. *J. Comput. Chem.* **1983**, *4*, 187−217.
(18) McMartin, C.; Bohacek, R. S. QXP: Powerful, rapid computer algorithms for structure-based drug design. *J. Comput.-Aided Mol. Des.* **1997**, *11*, 333−344.
(19) Figures 5, 9, and the TOC graphic were created using the program PyMOL.; Delano, W. L. *The PyMOL Molecular Graphics System*; DeLano Scientific LLC: San Carlos, CA. http://www.pymol.org.

JM050523N